Scanning Microscopy Vol. 12, No. 4, 1998 (Pages 535-552) 0891-7035/98$5.00+.25
Scanning Microscopy International, Chicago (AMF O'Hare), IL 60666 USA

THEORETICAL FUNDAMENTALS AND EXPERIMENTAL MATERIALS AND DEFECT STUDIES USING QUANTITATIVE SCANNING ELECTRON MICROSCOPY-CATHODOLUMINESCENCE/ELECTRON BEAM INDUCED CURRENT ON COMPOUND SEMICONDUCTORS

S. Hildebrandt*, J. Schreiber, W. Hergert, H. Uniewski and H. S. Leipner

Martin-Luther-Universität Halle-Wittenberg, Fachbereich Physik,
Friedemann-Bach-Platz 6, D-06108 Halle, Germany

(received for publication March 22, 1996 and in revised form February 27, 1997)

Abstract

The theoretical fundamentals for the calculation of the local cathodoluminescence (CL) signal and electron beam induced current (EBIC) in the scanning electron microscope (SEM) are outlined. Especially, the simulation of the signal contrast profile behavior of individual dislocation configurations is reviewed. Existing analytical models and new numerical approaches are summarized.

In addition to the evaluation of material parameters, the conception of combined SEM-CL/EBIC is applied to the quantitative experimental characterization of single defects in grown-in, misfit as well as glide dislocation structures with respect to their recombination activity in various III-V semiconductors. Recent CL data from dislocations in GaP, GaAs, and CdTe in the low-temperature range are analyzed in the framework of temperature-dependent defect-related recombination kinetics.

Key Words: Scanning electron microscopy, cathodoluminescence, electron beam induced current, compound semiconductors, III-V semiconductors, II-VI semiconductors, defects, dislocations, defect contrast, recombination activity.

*Address for correspondence:
S. Hildebrandt
Martin-Luther-Universität Halle-Wittenberg
Fachbereich Physik
Friedemann-Bach-Platz 6
D-06108 Halle, Germany
Telephone number: (+49) (3 45) 5 52 55 80
Fax number: (+49) (3 45) 5 52 71 58
E-mail: hildebrandt@physik.uni-halle.d400.de

Introduction

During the last decades, scanning electron microscopy (SEM) has been developed towards a standard experimental method to obtain images from a large variety of materials. In semiconductor characterization and research, the investigation of local electronic and optical properties is of vital importance for problems ranging from micro- and optoelectronic materials, devices, and quantum structures to solar cells. Here, both cathodoluminescence (CL) and electron beam induced current (EBIC) mode have been successfully applied [1, 3, 4, 25, 50, 59, 74] since they allow access to a defined specimen bulk region due to the beam-induced creation of electron-hole pairs. Besides the very important aspect of *imaging* and identification of particular features (electrically and optically active dislocations, precipitates, stacking faults, microdefects etc.) with high lateral resolution, *combined* SEM-CL/EBIC offers the possibility to determine reliable *quantitative* information on relevant local electronic and optical material parameters [39] and, especially, the recombination behavior at individual defects such as dislocations [62]. This purpose, however, requires an accurate simulation of the signals as a function of these parameters. The corresponding equations must also be related to the carrier recombination processes at the defect. Although this is a complex task in general, it may be largely simplified in many practical cases or even performed analytically. The appropriate model functions are then fitted to the experimental data, and the material parameter values are derived.

If we follow a strategic scheme for performing quantitative SEM-CL/EBIC investigations such as that given in Table 1, it is possible to obtain important information about the electronic properties and defect recombination activity which are significant for the treatment of many semiconductor defect physics problems. The suitability of the given strategy will be demonstrated by several theoretical and experimental examples in this paper. Some aspects of this scheme should be emphasized at this point. Investigations of the semiconductor matrix properties are a

Table 1. Strategy of SEM-CL/EBIC investigations on semiconductors

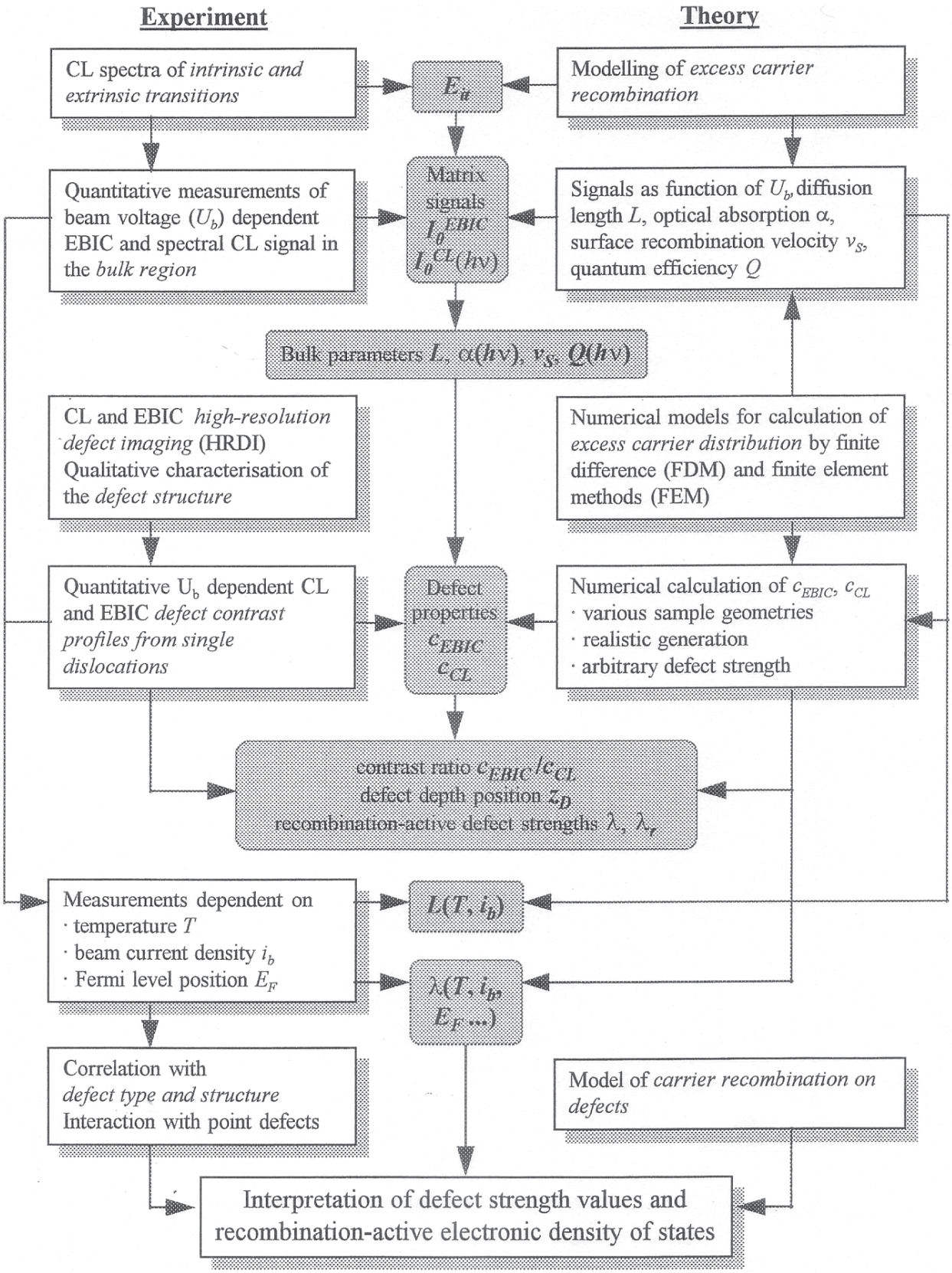

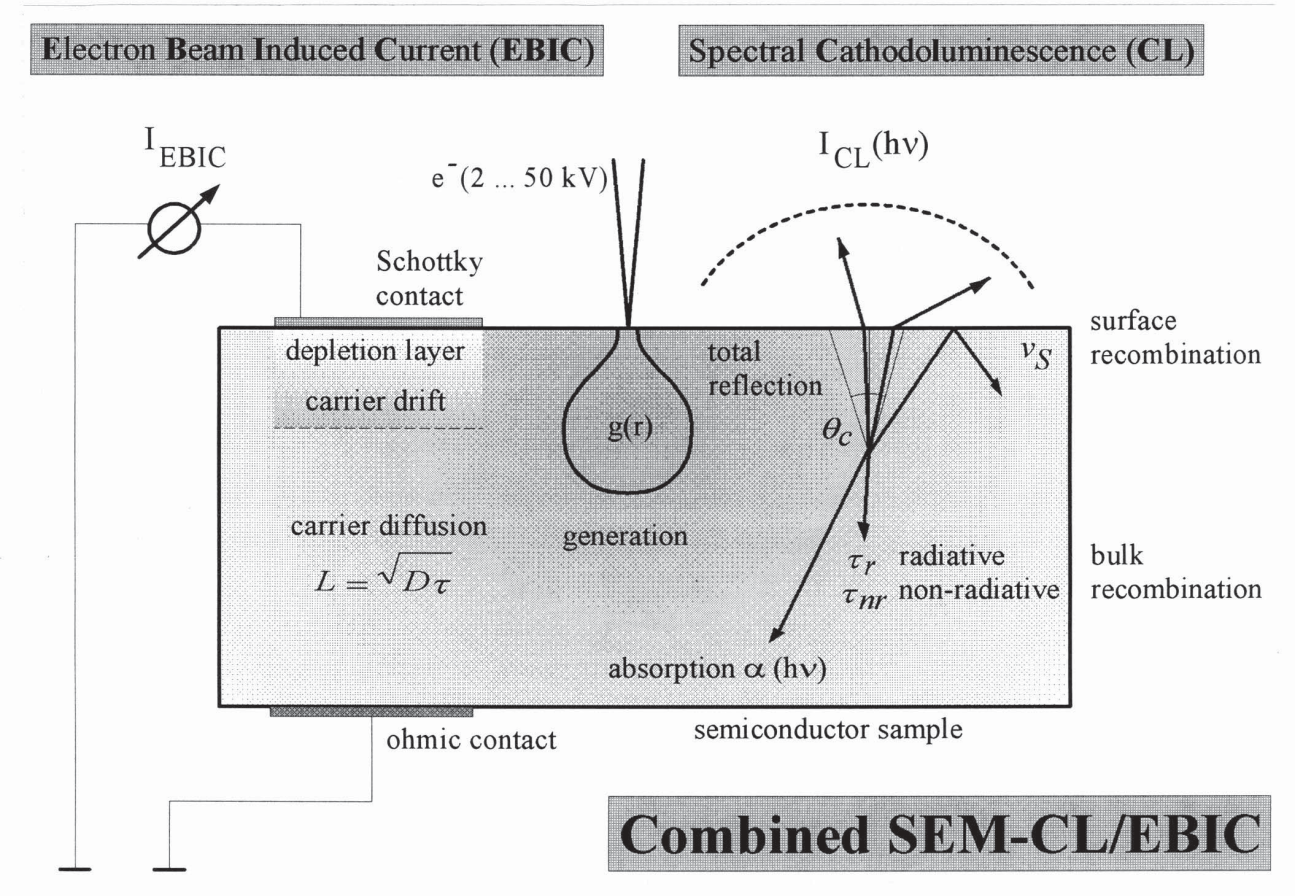

Figure 1. Scheme of combined SEM-CL/EBIC experiments.

necessary prerequisite for the quantitative study of defects and their electrical activity. Under these conditions, a complete set of matrix and defect parameters may be obtained from combined CL/EBIC measurements. This requires, however, comprehensive simulation models on one hand and information about the structure and configuration of the extended defects on the other. The knowledge about the carrier recombination processes is important for a correct interpretation of the experiments. While bulk recombination paths in semiconductors are generally known, the identification of the defect recombination mechanisms is a primary aim of these studies. Especially, the temperature dependence of dislocation recombination and the recombination kinetics when state occupation is changed by varying the injection level should be correlated with structural details such as the interaction with point defects and models about electronic states in the dislocation core and the surrounding region.

In this paper, we will restrict ourselves to an outline of the theoretical fundamentals for basic defect geometries such as a single dislocation in a thick epilayer or bulk sample with the aim of a *quantitative* experimental evaluation of corresponding model defect systems by *combined* CL and EBIC. We will follow the widely accepted generalized theoretical conception by Donolato, Pasemann, and Hergert [11, 14, 21, 28, 45, 47, 49]. The large variety of results from mainly qualitative investigations using CL or EBIC, detailed calculations for particular geometries as well as special aspects concerning quantum structures, devices or instrumentation are largely beyond the scope of our review. The interested reader is referred to some of the reviews cited above.

Theoretical Fundamentals

Figure 1 contains schematically the various carrier and photonic processes occurring in CL and EBIC experiments in the SEM. The carrier behavior is primarily represented by the electron-hole pair generation distribution $g(\boldsymbol{r})$, the minority carrier diffusion length $L=\sqrt{(D\tau)}$, and the radiative and non-radiative bulk lifetimes τ_r and τ_{nr} which determine the corresponding recombi-nation rates R_r and

R_{nr}. The continuity equation for the time-dependent excess minority carrier density $q(\boldsymbol{r},t)$ is established as the balance of diffusion and drift currents, total recombination, and beam induced generation rates at each point $\boldsymbol{r}$ of the sample:

$$-\frac{\partial}{\partial t}q(r,t)+D\nabla^2 q(r,t)-\mu\nabla\left(E(r,t)\,q(r,t)\right)-\frac{q(r,t)}{\tau(r)}=-g(r,t) \tag{1}$$

where the total minority carrier lifetime $\tau(\boldsymbol{r}) = (\tau_r^{-1} + \tau_{nr}^{-1})^{-1}$ is generally considered as a defect-related function of the location $\boldsymbol{r}$, D is the diffusion coefficient, and μ the minority carrier mobility. The validity of 0 requires a linear recombination model such as band-to-band recombination in the low-injection regime (e.g., $q = \Delta p \ll n_0$ for an extrinsic n-type semiconductor) so that the majority carriers do not need to be considered. If electric fields $E(\boldsymbol{r},t)$ can be neglected in a neutral bulk semiconductor, the stationary balance ($\partial p/\partial t = 0$) is described by the steady-state continuity diffusion equation

$$D\nabla^2 q(r)-\frac{1}{\tau(r)}q(r)=-g(r)\ . \tag{2}$$

According to the actual sample geometry, boundary conditions have to be fulfilled such as

$$D\left.\frac{\partial q}{\partial n}\right|_{r=r_s}=\nu_s\,q(r_s) \tag{3}$$

for any surface or interface $\boldsymbol{r}_S$ where a normal diffusion current is linked to a non-radiative surface/interface recombination velocity v_S. In directions with practically infinite sample extensions, the carrier density must vanish ($q(\boldsymbol{r}) \to 0$ for $\boldsymbol{r} \to \infty$).

For the generation rate, various models have been used in the literature. For the given partial differential equation of Helmholtz type, a delta-function point source leads to the determination of Green's function $G(\boldsymbol{r},\boldsymbol{r}')$. It can be obtained using the method of mirror images [11] for various defect-free sample geometries. Due to its mathematical simplicity, a uniform sphere generation also allows the determination of $q_0(\boldsymbol{r})$ for the homogeneous half-infinite sample in analytical form [22]. For a correct quantitative analysis of experimental data, however, the use of a *realistic* generation distribution $g(\boldsymbol{r};U_b) = G_0\, g_r(r,z)\, g_z(z)$ is essential (G_0 is the total carrier generation rate). It can be obtained by Monte Carlo (MC) simulation of scattering and energy dissipation of primary electrons of energy eU_b inside the sample [70]. The versatility and simplicity of MC generation models favor their universal application even in complex geometrical cases [7, 56]. To obtain accurate results, however, they may demand long computation times. Since it would complicate a fast analysis if the same task had to be repeatedly solved for equivalent experimental conditions on bulk materials, an empirical three-component Gaussian expression has been accurately fitted to MC results once calculated in the beam voltage range U_b = 2 ... 50 kV and semiconductor materials with average atomic number between Si and GaAs [38, 61, 70]. Furthermore, for the exact modelling of EBIC and CL signal from the homogeneous matrix region (see below) as well as the defect contrast profile area of a surface-parallel dislocation [27], only the well-known depth distribution $g_z(z;U_b)$ (see eqn. 0) and no explicit calculation of $q(\boldsymbol{r})$ is required. For these reasons, the effort of repeated MC simulations is often unnecessary, and it can be separated from the actual problem of signal modelling. This fact is sometimes ignored in the literature [9, 31, 54].

Finally, by choosing the appropriate light generation function, the considerations of this paper may be readily applied to light beam induced current (LBIC) and photoluminescence (PL) which might be very useful in view of the recent progress in scanning PL investigations of dislocations [68].

In order to perform an EBIC experiment, the sample must contain a potential barrier to separate the generated electron-hole pairs such as the surface Schottky barrier of Figure 1or a p-n junction so that the major part of the EBIC signal is given by the diffusion current towards the edge of the depletion region $\boldsymbol{r}_b$ [11]:

$$I^{EBIC} = e\,D\iint\limits_{r=r_b} dA\,\frac{\partial q(r)}{\partial n}\ . \tag{4}$$

An additional drift current contribution may originate from the separation of carriers generated inside the depletion layer.

The spectral CL signal (photon flux leaving the sample surface) collected by an ideal spectrometer [22]

$$I^{CL}(h\nu) = Q(h\nu)\int\limits_0^{\Theta_c} d\Theta\sin\Theta\int\limits_{\Omega_s} d^3r\,\frac{q(r)}{\tau_r}\exp\left(-\frac{\alpha(h\nu)z}{\cos\Theta}\right) \tag{5}$$

is given by the integral of the *radiative* recombination rate over the sample volume Ω_s corrected by losses due to spectral optical absorption $\alpha(h\nu)$ and total reflection at the

[1] Effects of reabsorption of recombination radiation [39, 57], i.e., renewed generation of electron-hole pairs by photon absorption, are neglected throughout this paper.

sample surface for escape angles larger than the critical angle Θ_c. $Q(h\nu)$ denotes the relative internal spectral distribution of the recombination radiation. In the case of panchromatic, spectrally integrated CL experiments, equation (5) remains correct if "effective" parameters for quantum efficiency $\overline{Q}$ and absorption $\overline{\alpha}$ are introduced.

An important advantage for the calculation of the matrix signals from a defect-free region was the introduction of a unified formalism [21] being valid for all sample geometries with rotational symmetry. Induced current and luminescence signals are expressed in terms of a universal function describing the specific exponential losses by diffusion or absorption and the effect of an *arbitrary* generation depth distribution:

$$\Phi(x, z_1, z_2; U_b) = \int_{z_1}^{z_2} dz\; g_z(z; U_b) e^{-x(z - z_1)} \quad . \tag{6}$$

For example, we obtain a simple formula for the CL signal from a semi-infinite homogeneous sample with a dead layer of thickness z_T at the surface ($S = \nu_s \tau / L$, $\hat{\alpha} = \alpha / \cos\theta$)

$$I_0^{CL}(hny; U_b) \propto Q(hny) \int_0^{\Theta_c} d\Theta \frac{\sin\Theta\, G_0 e^{-\hat{\alpha} z_T}}{1 - \hat{\alpha}^2 L^2} \times \times \left[\Phi(\hat{\alpha}, z_T, \infty; U_b) - \frac{\hat{\alpha} L + S}{1 + S} \Phi\left(\frac{1}{L}, z_T, \infty; U_b \right) \right] \quad . \tag{7}$$

Similar expressions are derived for the surface-parallel Schottky or p-n EBIC signal with explicit consideration of metal and/or depletion layers as well as for layered structures [21, 43]. Many other literature results such as [10] could be covered more easily within this framework as well. It should be noted that the so-called normal collector geometry with a p-n or heterojunction perpendicular to the surface has a more complicated solution which will not be discussed here (see, for example [13, 18, 42, 44]).

In connection with the calculation of the matrix signals using the unified formalism, the concept of information depth z_I and information radius r_I, i.e. the range where 95 % of the CL radiation originate from, has been developed [20, 22]. It was found that $z_I \approx 4$ µm for $\alpha > 10^4$ cm^{-1}, $L > 1$ µm nearly independent of U_b. Other ways to determine the lateral image resolution in EBIC and CL have been proposed in [12, 51].

For comprehensive studies on the formation of the defect contrast from dislocations it is necessary to take into account the intrinsic nature of dislocation recombination, effects due to interaction with surrounding point defects as

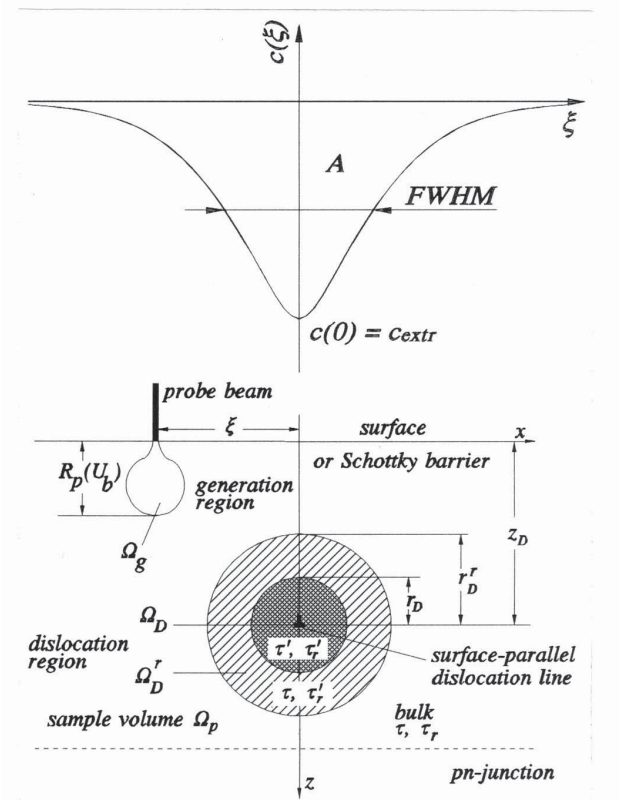

Figure 2. Schematic configuration of CL/EBIC contrast measurements at a surface-parallel dislocation.

well as geometric contrast factors. Generally, defects are supposed to change the local recombination properties of the sample. Hence, their electric activity resulting in a recombination contrast has to be considered with respect to bulk recombination rates. The knowledge of matrix signals and corresponding parameters is therefore a general requirement for a quantitative analysis of the defect contrast. In our fundamental considerations we will mainly refer to the model case of a surface-parallel dislocation applicable for many both misfit and glide dislocation geometries (Figure 2). Beyond the basic configurations of single surface-parallel or -perpendicular dislocation lines, the large variety of possible situations such as inclined, curved, or composed defect features should be the subject of numerical modelling (cf. below).

In the *volume recombination model* (VRM), the dislocation is characterized by a cylindrical region Ω_D where the total lifetime τ' differs from the bulk value τ. The defect-induced *recombination strength* [11] is given by

$$\gamma = \tau/\tau' - 1 = \tau/\tau_D \tag{8}$$

The radius r_D of the dislocation cylinder may be first

interpreted as a "capture cross section" but one can also try to infer this region from physical dislocation properties such the extension of the core region, strain field or the space charge region of a charged dislocation. However, it can be shown that for $r_D \ll L$ the shape of the contrast profile of a surface-parallel dislocation line is independent of r_D. In this case, γ and r_D cannot be determined separately but form together a *defect strength* λ [41[2], 45] (cf. eqn. 0). On the other hand, impurity decoration or a gettering-induced denuded zone may cause a larger extension of the defect-related region as shown e.g. for GaAs in an early work by Balk *et al*. [3]. In such a situation or if specific defect bound emission occurs, the radiative recombination can be directly affected. This is considered by introduction of a second defect cylinder $\Omega_D{}^r$ of radius $r_D{}^r$ with modified τ_r' and $\gamma_r = \tau_r/\tau_r$' - 1, respectively. In principle, this model is able to describe the well-known "dot-and-halo" contrasts.

It is noted that in the alternative "surface" recombination model [34] the dislocation is represented by a recombination velocity at the cylinder boundary instead. This model may yield partly analogous results as the VRM, however, it will deviate if defect and generation region overlap each other - a common experimental situation - since this would result in an unrealistic 100 % contrast contribution from this region. These difficulties could be overcome by the introduction of an "effective" radius [34].

A defect *contrast profile*, i.e. the linescan over the defect, is given by

$$c(\xi) = \frac{I(\xi) - I_0}{I_0} \quad , \quad I_0 = I(\xi \to \infty) \tag{9}$$

where ξ is the lateral beam position relative to the defect and I_0 the matrix signal far away from it. Usually, the central value $c(0)$ is denoted "the (maximum) contrast value" irrespective of its sign (here defined negative for a dark and positive for a bright image contrast). Furthermore, the profile half-width (FWHM) and the contrast profile area [15, 27] may be used to characterize the contrast.

The CL defect contrast has been derived [49, 59] as

$$c_{CL} = \int_0^{\Theta_c} \frac{d\,\Theta \sin\Theta}{\tau_r I_0^{CL}} \left[-\gamma \int_{\Omega_D} d^3 r\, q(r)\, j_0^{CL}(z) + \gamma_r \int_{\Omega_D^r} d^3 r\, q(r) e^{-\hat{\alpha} z} \right]. \tag{10}$$

Here, $j_0{}^{CL}(z)$ stands for the defect-free CL signal from a point source located at depth z. According to the cylindrical regions in the VRM, it generally consists of two parts. The first part arises from the change in the total lifetime and is analogous to the EBIC contrast expression not written here. The second, CL-specific term results in an exclusive luminescence contrast contribution caused by the change of τ_r at the defect provided the total lifetime τ remains unaffected by the variation in τ_r.

Obviously, the central task of the contrast calculation is the determination of the carrier density $q(\boldsymbol{r})$ in the sample containing the defect. It is related to the defect-free case $q_0(\boldsymbol{r})$ by the Dyson integral equation

$$q(r) = q_0(r) - \frac{\gamma}{4\pi L^2} \int_{\Omega_D} d^3 r'\, G(r, r')\, q(r') \quad . \tag{11}$$

A common method for the analytical solution of equation 0 is perturbation theory. In first order [11], the undisturbed $q(\boldsymbol{r}) = q_0(\boldsymbol{r})$ can be used for the calculation of the contrast of weak defects. $q_0(\boldsymbol{r})$ is known analytically for uniform sphere generation [22] and can be calculated half-numerically for a realistic generation in a half-infinite sample with $S \to \infty$ [28].

Although nowadays the entire contrast simulation could be performed numerically [9, 31, 52, 53, 69] analytical methods are of great value. Besides their smaller computational effort, they allow better insight into contrast formation and properties. In this way, it was realized that the contrast of a surface-parallel dislocation may be written as [28, 60]

$$c_{EBIC}(\xi, U_b) = \lambda c^*_{EBIC} \approx \lambda\, f_0^{EBIC}(L' z_D; U_b)\, c^{**}(\xi, L, z_D; U_b) \tag{12a}$$

$$\begin{aligned} c_{CL}(\xi, U_b) &= \lambda\, c^*_{CL} + \lambda_r\, c^{*,r}_{CL} \\ &\approx \lambda\, f_0^{CL}(L, \alpha, z_D; U_b)\, c^{**}(\xi, L, z_D; U_b)(\lambda_r = 0) \end{aligned} \tag{12b}$$

that means in terms of products of a function c* and a corresponding defect strength λ or λ_r. We note that if $\lambda_r = 0$, both EBIC and CL contrast profiles are given by the same profile shape function c** and only the contrast amplitudes differ according to f_0^{EBIC} and f_0^{CL}.

In *first order* perturbation theory we obtain for the *total* and *radiative defect strength*, respectively,

$$\lambda^{(1)} = \gamma \pi (r_D/L)^2 \,, \; \lambda_r^{(1)} = \gamma_r \pi (r_D{}^r/L)^2 \quad . \tag{13}$$

The further perturbation expansion has been evaluated in [45] leading to modified defect strength expressions. It was found that the series converges for $\lambda^{(1)} < 1.2$ only. The convergence criteria were discussed in [23]. However, the

[2] In [41], however, an incorrect formula for the CL intensity was used.

theoretical contrast description must be able to cover a wide range of defect strength values. Strongly recombination-active defects cause a noticeable change in the excess minority carrier density giving rise to a complex non-linear contrast behavior with saturation of the diffusion controlled recombination for high activity. Several approaches were developed for a contrast solution valid beyond the convergence domain [14, 47, 62] as illustrated in Figure 5. Therefore, the problem of calculation of CL and EBIC contrast from a surface-parallel dislocation may now be considered as completely solved.

Finally, we can see from equations 0 and 0 that for $\lambda_r = 0$, $r_D \ll z_D$,L the *contrast ratio* c_{EBIC}/c_{CL} is given by f_0^{EBIC}/f_0^{CL} being an exact measure of the depth position z_D of the surface-parallel dislocation line, dependent on the matrix parameters only [49]. This property caused by the complementary response of EBIC and CL signal to the spatial propagation of charge carriers and recombination radiation is of great practical use for the determination of defect depths and a complete contrast analysis requiring the knowledge of z_D.

For a surface-perpendicular dislocation, the theorem of reciprocity allows a rigorous calculation of c_{EBIC} as an integral expression for arbitrary generation [46]. It is an elementary property of Green's function[3] which connects the EBIC signal (the diffusion current) in the case of carrier generation by a point source at $\boldsymbol{r}$ with the reciprocal case of homogeneous injection of $\overline{n}$ carriers over the EBIC barrier to produce a minority carrier distribution $n(\boldsymbol{r})$ in the sample:

$$I^{EBIC}(r) = G_0 \frac{n(r)}{\overline{n}} \ . \qquad (14)$$

It was shown that contrary to the surface-parallel line defect, for very low values of U_b (electron range $R_p \leq 2\, r_D$) $l^{(1)}$ is not a suitable recombination activity parameter since various combinations of t/t' and r_D give divergent contrast curves and profile half-widths. Although this particular half-width behavior might be helpful for a direct estimate of the defect radius r_D, it has not been proved experimentally yet. It may be expected that depletion region and surface recombination effects will also influence the EBIC contrast. Therefore, we will not further discuss this situation in the paper. The reciprocity concept is not simply transferable to the case of CL. In order to treat this case as well as other dislocation geometries such as inclined dislocations [69], new findings are expected from results of numerical calculations.

[3] In electrostatics, the theorem of reciprocity describes the equality of the charge induced on a grounded conductor by a unit point charge at $\boldsymbol{r}$ with the corresponding potential in $\boldsymbol{r}$ if a unit potential is applied to the conductor.

Simulation Results

Results of simulations of the matrix signals I_0^{EBIC} and I_0^{CL} from defect-free samples can be found in [24, 37, 73]. It was shown that the beam-voltage dependent Schottky-EBIC signal $I_0^{EBIC}(U_b)$ plotted for constant G_0 is sensitive to the diffusion length as well as to the metal layer thickness z_m. For the surface-parallel p-n geometry and layered structures or inhomogeneous material, depth profiles of L can be extracted [16]. The corresponding CL signal depends on S and z_T but it is dominated by the diffusion length L and the optical absorption $\alpha(h\nu)$ or $\overline{\alpha}$, respectively. Both parameters exhibit a strong correlation in the signal. In order to prevent the evaluation of ambiguous values, the maximum position U_b^{max} of $I_0^{CL}(U_b)/G_0$ may be used to estimate α [24] if L is known from other experiments such as simultaneous EBIC measurements, for instance using a thin transparent Schottky contact ($z_m \approx 10$ nm) on the surface. The CL mode also permits to locate lateral and vertical inhomogeneities or buried interfaces if a suitable model can be applied [8, 35]. Normal-collector EBIC line profiles allow to determine the diffusion lengths L_n and L_p on both sides of the p-n junction as well as S [13, 18].

CL and EBIC dislocation contrasts show a characteristic behavior as a function of the beam voltage. The typical behavior for a surface-parallel dislocation is illustrated in Figure 3. Since the contrast value is strongly influenced by geometric factors such as generation range $R_p(U_b)$ and defect depth z_D, the evaluation of the recombination activity is only possible if these parameters are known. If both EBIC and CL contrast can be measured, the contrast ratio c_{EBIC}/c_{CL} yields z_D. Consequently, a combined CL/EBIC experiment at one given beam voltage would be sufficient to determine λ. However, a complete measurement of the $c(U_b)$ curve yields more reliable data, and the depth position may then also be derived as an additional fit parameter (cf. Figure 8). Arising from the joint profile function c^{**}, profile half-widths of CL and EBIC contrast are identical. Plotted in Figure 3(b), they do not exhibit a minimum as predicted for uniform sphere generation [11] but rise from a nearly constant value with increasing U_b. For shallow dislocations, the gradual decrease at high U_b beyond the maximum half-width is a special feature of the realistic generation in accordance with [53] and own, unpublished experimental data from GaAsP.

An example for the influence of the matrix parameters on the contrast profiles is shown in Figure 4. It is seen that a variation of the bulk diffusion length results in rapid changes in maximum contrast and profile half-width predominantly in the range $L \approx 1$ µm. This behavior may be

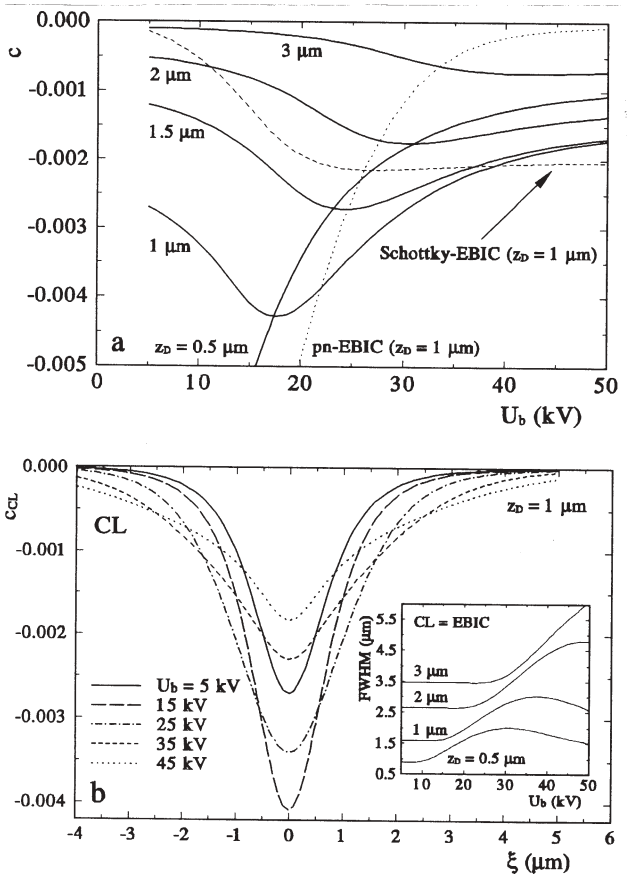

Figure 3. (**a**) Calculated CL contrast from a surface-parallel dislocation for various depths z_D (L = 1 µm, α = 0.75 µm^{-1}, $S \rightarrow \infty$, λ = 0.01 π, λ_r = 0). For z_D = 1 µm, Schottky and p-n EBIC contrasts are also shown. (**b**) Corresponding contrast profiles at z_D = 1 µm. The inset shows CL/EBIC profile half-widths as a function of U_b and z_D.

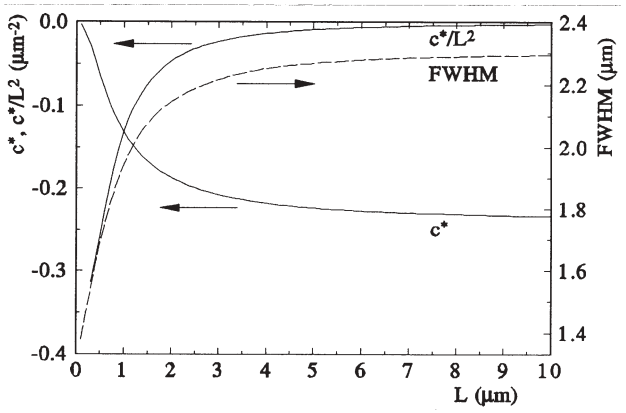

Figure 4. CL contrast profile function and half-width for varying L (α = 0.75 µm^{-1}, $S \rightarrow \infty$, r_D = 0.1 µm, λ_r = 0, z_D = 1 µm, U_b = 20 kV). Both $c_{CL}^* \sim c$ for constant λ = 0.01 π and $c_{CL}^*/L^2 \sim c$ for constant γ = 1 are shown.

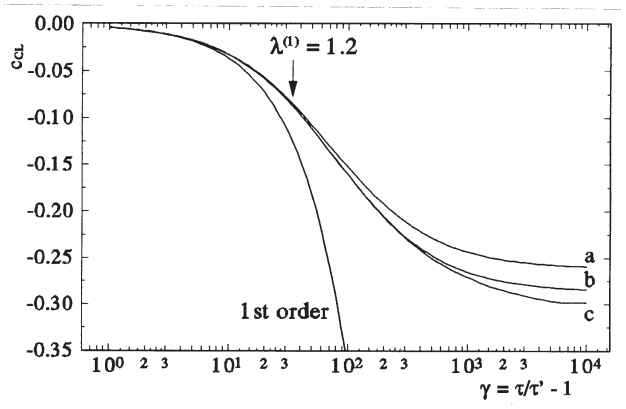

Figure 5 (after [62]). CL contrast for varying recombination strength γ (L = 1 µm, α = 0.75 µm^{-1}, $S \rightarrow \infty$, r_D = 0.1 µm, λ_r = 0, z_D = 1 µm, U_b = 20 kV) (a) analytical approximation [62], (b) series expansion [45], (c) rotation-symmetric solution [14]

important for the interpretation of temperature-dependent contrast measurements on III-V materials as discussed below. Only for large L > 5 µm (typical for Si), the influence of the diffusion length is small and a constant half-width is found.

We expect from equation 0 that λ may be obtained from a comparison of the experimental contrast and the theoretical profile function which can be calculated if the other parameters are given. However, the defect strength determined in this way cannot grow arbitrarily high. Even if a defect is considered as a "black sphere" (τ' = 0), the contrast will not range above a saturation value [14] due to the defect-induced local reduction of $q(\boldsymbol{r})$. An example for this contrast property is shown in Figure 5. The first order approximation 0 is applicable only for weak defects $\lambda^{(1)} <$ 0.15. Although there is some variation between the various other models they all show basically the same saturation behavior for high γ (including the sum of the perturbation expansion which actually holds for $\lambda^{(1)} < 1.2$ only). It should be further noted that the *shape* of the contrast profile remains unaffected by the γ value.

It is thus concluded that λ has to be generally interpreted as a *non-linear defect strength* being the appropriate parameter for the quantitative description of the specific dislocation recombination activity in CL/EBIC experiments. A direct relation to the defect-induced lifetime ratio or recombination rate is only possible for the case of a weak defect or otherwise if the degree of deviation from linearity is known, for instance if an estimate for r_D can be given [69].

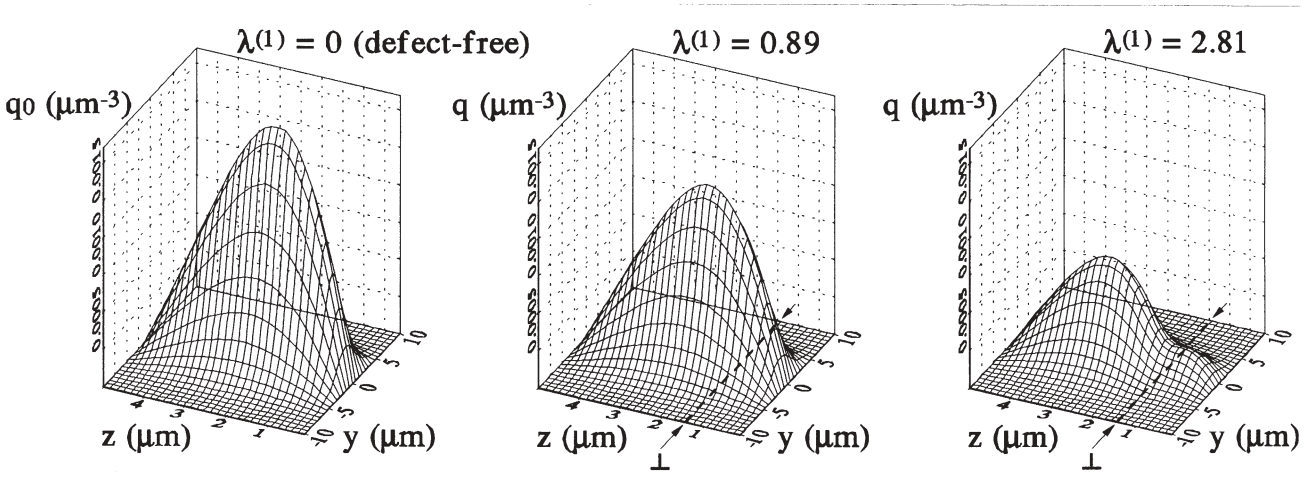

Figure 6. Numerically calculated excess carrier density $q(0,y,z)$ for various defect strengths of a surface-parallel line defect (position denoted by arrows) in a 5 μm thick layer (L = 3 μm, $S \rightarrow \infty$, z_D = 1.43 μm, U_b = 20 kV, ξ = 2.9 μm)

During the last years, increased efforts have been made to develop *numerical* simulation models for the calculation of the excess carrier distribution, CL and EBIC signals, and the defect contrast [9, 31, 36, 52, 53, 69]. Numerical methods have the advantage of being able to deal with defects with irregular shapes and characteristics.

In the framework of the above given model, arbitrary defect and sample geometries may be treated by a finite difference scheme. A first result for the numerical simulation of $q(\mathbf{r})$ in the presence of a surface-parallel dislocation line using the realistic generation model is presented in Figure 6. For these calculations, the FIDISOL/CADSOL solver is conveniently applied [58], a program package developed for the solution of boundary value problems for systems of partial differential equations of various types using a nonequidistant grid and varying order of consistence. Grid size and spacings have to be chosen carefully in order to minimize numerical errors and to model the defect with sufficient precision. It is clearly seen from the results in which way $q(\mathbf{r})$ is modified by the action of the dislocation. For small defect strengths ($\lambda^{(1)} = 0.89$), the carrier density is reduced but its original shape is maintained. This explains why in this range the undisturbed distribution $q_0(\mathbf{r})$ may be used in first order analytical calculation. Only for higher defect strength values, the *local* distortion of $q(\mathbf{r})$ around the defect becomes significant. CL and EBIC signals and contrasts may be reproduced by numerical integration/ differentiation of the carrier density choosing either the full calculation by eqns. 0 and (5) or the contrast formula (eqn. 10).

Despite the fast advances in available computing capacity, a full numerical treatment of the spatial carrier behavior still needs high memory and time requirements. The general problem of the solution of the coupled basic electronic and transport equations is rather extensive and closely related to complex tasks in device simulation [36, 64]. We conclude here that these methods exhibit a big potential, however, it should be considered which cases really require a numerical treatment. The symmetry of the problem as well as the fact that the calculation of the contrast (eqn. 10) requires that $q(\mathbf{r})$ *only inside the defect region* should be taken into account. Furthermore, alternative ways in contrast modelling such as finite element techniques could be used where body-oriented grids can be more easily adapted to defect and generation geometries.

Experimental Details

For the performance of CL and EBIC experiments, the SEM should permit a beam voltage variation from below 1 kV up to high values of at least 40 kV. The range between 40 and 50 kV which is accessible using our SEM Tesla BS 300 is, however, hardly offered by commercial suppliers today. The electron gun (preferably LaB_6 cathode) and optics must be able to supply small stable beam currents to ensure low injection conditions with beam powers of $U_b I_b < 20$ μW over the whole U_b range. Beam currents are measured using a Faraday cup. Small luminescence intensities require an efficient, optimized collection system with a parabolic or elliptic mirror and photomultiplier or Si diode detectors. For the spectroscopic CL investigations, we use narrow band pass filters or a grating spectrometer system (CL302m from Oxford Instruments, Oxford, UK). Lock-in amplification, optical multichannel analyzers, or

Boxcar technique in combination with digital scan for EBIC and panchromatic or monochromatic CL line profile recording as well as image processing are widely available now. The temperature-dependent studies are performed under vacuum conditions of better than 10^{-4} Pa in the temperature range between 5 and 300 K in the SEM equipped with liquid helium or nitrogen cooling stage (CF 302 by Oxford Instruments in our setup).

Samples are epitaxial and bulk material of (001) or (111) orientation. For glide dislocation generation, plastic microdeformation is achieved by Vickers indentation at room temperature with typically 0.05 to 0.4 N load to activate the principal {111}⟨110⟩ glide systems. For GaAs, it is followed by a thermal treatment of 15 min at 400°C. The qualititative characterization of the defect configuration is performed by means of crystallographic considerations of the dislocation rosette geometry or by transmission electron microscopy (TEM) investigations. Semitransparent Au Schottky contacts on n-type III-V sample surfaces are produced by vacuum evaporation using standard preparation methods. For ohmic contacts, an Au-Ge eutectic on the sample backside is annealed at 350°C for 10 min.

Experimental Results

It has been demonstrated in a number of papers how material parameters such as L, α, and Q in compound semiconductors can be determined from fits to EBIC and CL data of homogeneous sample regions based on the results of the theoretical simulation. In order to investigate the recombination mechanisms in optoelectronic materials, the parameter variation with doping level in bulk n-GaAs (n_0 = $7 \cdot 10^{16}$ to $3 \cdot 10^{18}$ cm^{-3}) [39, 55] and GaAsP was studied using EBIC and *panchromatic* CL. The diffusion length $L(n_0)$ does not always show a systematic doping dependence. However, because of $\tau_r \sim n_0^{-1}$ and $L^2 \sim \tau$ (D = const.) the relation for the relative quantum efficiency $Q(n_0) \sim n_0 L^2$ was shown to be in good agreement with the experiment. It could be verified that the recombination is dominated by non-radiative processes $\tau \approx \tau_{nr}$ except near the maximum of Q at $n_0 \approx 10^{18}$ cm^{-3} where τ_r and τ_{nr} become comparable. Panchromatic CL measurements allow to determine only an effective absorption coefficient $\overline{\alpha}$. It decreases with doping according to the Burstein-Moss shift of the absorption edge to higher energies relative to the spectral position of the CL band.

More detailed information about material properties may be derived from *spectrally resolved* CL data $I_0^{CL}(h\nu;U_b)$ [29]. Figure 7(a) shows an example for the monochromatic beam voltage dependencies converted from CL spectra of p-GaAs measured at constant beam power $U_b I_b$ = 20 µW. They display a clearly variable shape with photon energy $h\nu$. The spectral absorption edge $\alpha(h\nu)$ may be accurately

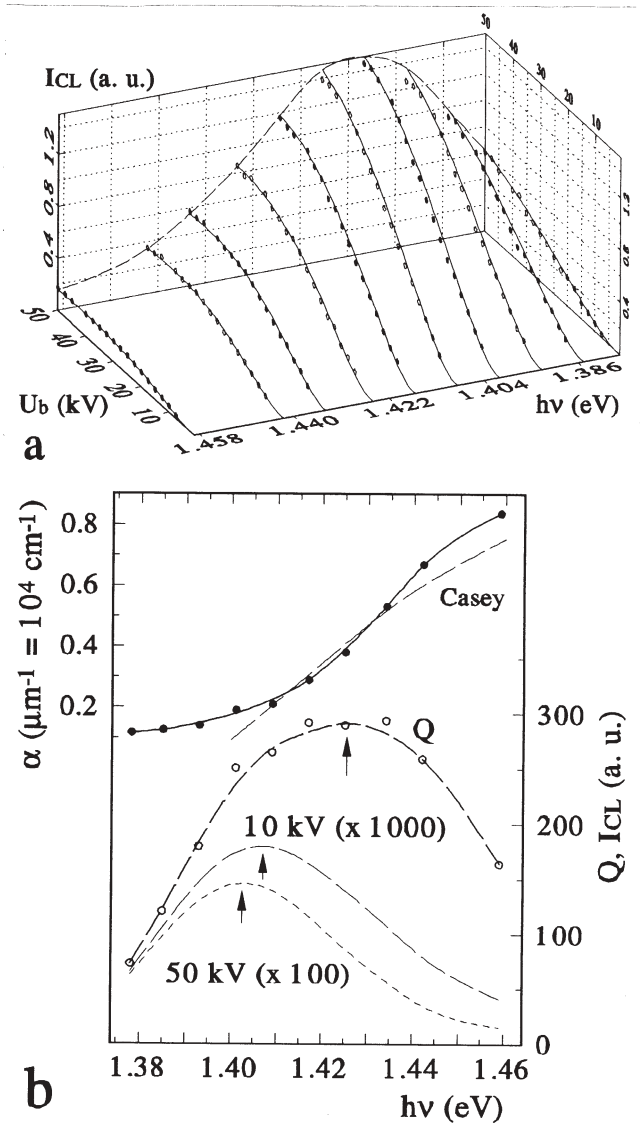

Figure 7 (after [29]) (**a**) Experimental and fitted spectral CL signal ($U_b I_b$ = 20 µW) from p-GaAs (L = 4.5 µm, z_T = 0.07 µm, $S \rightarrow \infty$), (**b**) Fit results. Top: Absorption coefficient compared with [6], bottom: Internal spectral distribution and measured CL spectra at U_b = 10 kV and 50 kV. Arrows denote the spectral maximum positions.

determined by the fit (Figure 7 (b)). Because of the large electron diffusion length L = 4.5 µm in the p-type material as determined by EBIC, the CL intensity increases rather slowly with U_b. Therefore, the absorption-related signal maximum is expected beyond 50 kV in this example. However, due to the large extension of the diffusion region, the absorption still plays a significant role even at 10 kV causing a low-energetic shift of the CL spectrum by about 20 meV compared to the *internal* spectral distribution $Q(h\nu)$. This emphasizes

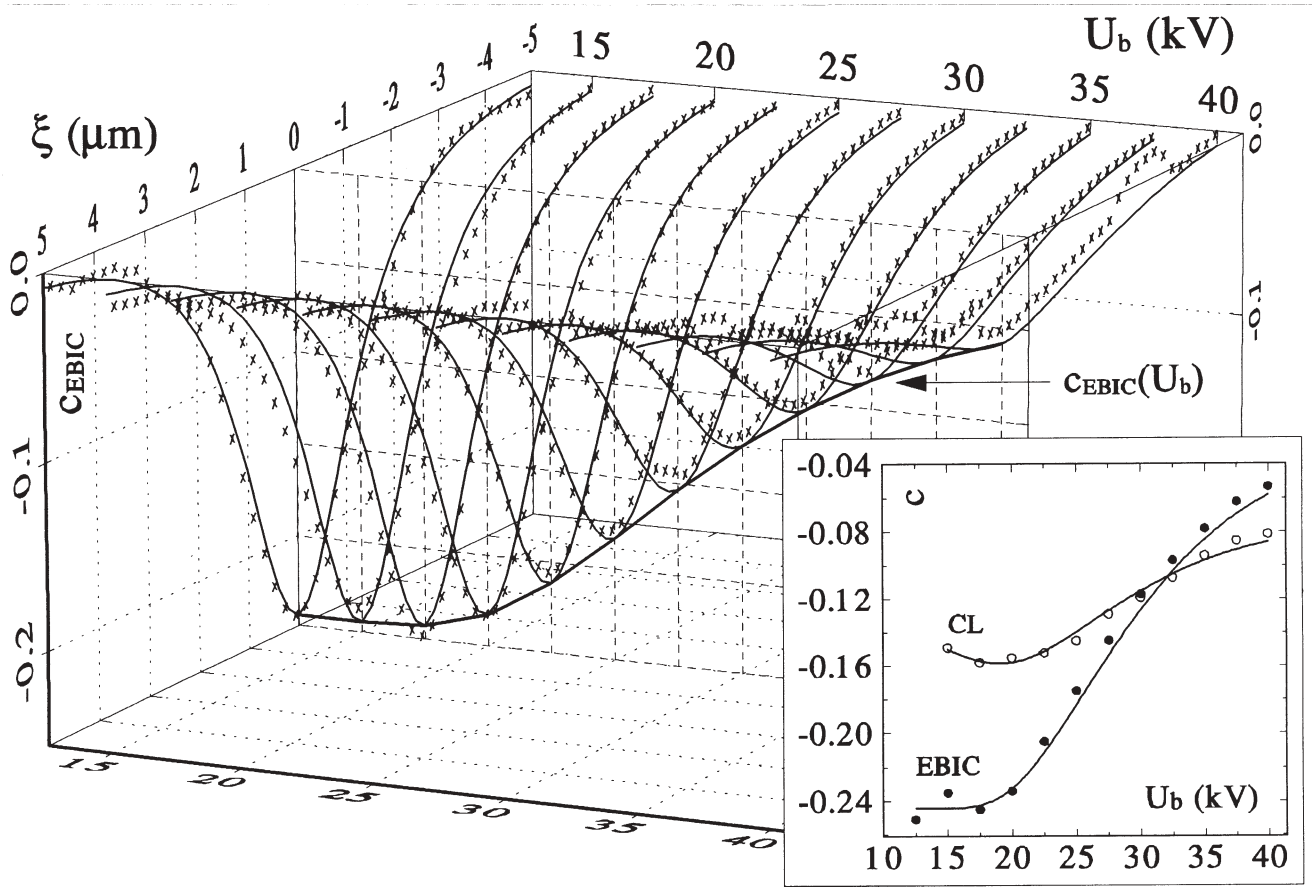

Figure 8 (after [61]). Experimental EBIC contrast profiles and best fits for a surface-parallel dislocation in p-GaAs ($\lambda = 0.89$, $z_D = 1.43$ μm, $L = 3.0$ μm). The inset shows the experimental and fitted EBIC and CL maximum contrast ($\lambda_{CL} = 0.73$).

the advantage of spectral CL experiments for the determination of the absorption edge and self-absorption correction.

For the quantitative investigation of single defects, the conception of combined beam-voltage dependent CL and EBIC contrast profile measurements has been successfully applied to dislocations in GaAs, GaP, and GaAsP by the authors [59, 60, 61, 62]. Other workers [32, 33] have also investigated either $c_{EBIC}(U_b)$ or $c_{CL}(U_b)$ without detailed evaluation of the recombination activity. Figure 8 displays results of contrast measurements from a process- or stress-induced surface-parallel dislocation in the near-surface p-type region of a GaAs p-n diode structure. Using the realistic generation function with depth-dependent half-width of the radial distribution $g_r(r,z)$ [38], excellent fits to both the maximum contrast and the contrast profiles were achieved over the whole beam voltage region. The dislocation depth is in agreement with the value given by the EBIC/CL contrast ratio. Obtained differences between defect strength values derived from EBIC and CL, respectively, discussed in [61] could be attributed to a locally changed background CL intensity due to the gettering activity of the dislocation.

A comparison of CL defect contrasts from an edge-type misfit dislocation in $GaAs_{0.38}P_{0.62}$ and a screw-type glide dislocation in GaAs is shown in Figure 9. Both defects exhibit the same basic homogeneous, dark contrast appearance. The maximum contrasts as well as the profile half-widths between 1.5 and 3.5 μm are in good correspondence to the results of the model calculations with minimum FWHM for both examples. Spectroscopic CL investigations show no variation in the spectral distribution from defect and matrix regions. The observed noticeable differences in recombination activity between grown-in defects and dislocations freshly introduced by microdeformation should therefore be attributed to the intrinsic dislocation behavior or to the influence of a rather weak impurity or point defect decoration. These two cases can only be distinguished by

Table 2. Defect strength values of dislocations in semiconductors

Material	Defect type	L (μm)	z_D (μm)	λ
n-GaP ($n_0 = 9 \cdot 10^{17}$ cm^{-3}) [62]	60°/90° misfit dislocation	0.89	1.05	2.45
n-$GaAs_{0.62}P_{0.38}$:Te ($n_0 = 3 \cdot 10^{16}$ cm^{-3})	60°/90° misfit dislocations	0.90	0.77 ... 2.02	1.26 ... 1.78
p-GaAs:Zn ($p_0 = 10^{18}$ cm^{-3}) [61]	process-induced edge dislocation (several positions)	3.05	1.43	0.68 ... 1.27
n-GaAs:Si ($n_0 = 9 \cdot 10^{17}$ cm^{-3})	screw glide dislocations	0.73	1.13 ... 1.58	0.58 ... 0.95
GaAs:Si ($n_0 = 1 \cdot 10^{17}$ cm^{-3}) [69]	screw glide dislocation	1.6	0 ... 0.7 (inclined)	0.89[1]
n-GaAs:Si ($n_0 = 4 \cdot 10^{16}$ cm^{-3}) [72]	60°-α glide dislocation	1.4	(45° inclined)	1.22[2]
p-Si[3] [48]	60°	1.5	1.60 ... 1.90	0.68
	60° (dissociated)	1.5	1.60 ... 1.80	0.29
	screw	1.5	1.35	0.02

[1]calculated for $z_D = 0.5$ μm, $r_D = (50 \pm 25)$ nm, $\tau' = 7.4$ ps, $\tau = 4.1$ ns measured on 2.2° inclined dislocation configuration.
[2]calculated for $z_D = 0.5$ μm, $r_D = 45$ nm, $\tau' = 2$ ps, $\tau = 2.2$ ns estimated from DLTS and EBIC experiments.
[3]results from diffusion-induced dislocations in Si given for comparison.

further experiments such as recombination-kinetic studies (see below). Strong decoration effects, however, may be excluded here. It is noted that a quantitative evaluation of the recombination activity is only possible by using the fitted λ values but not by comparing the contrast values which are strongly dependent on U_b and z_D.

Representative defect strength results are compiled in . A wide range of λ values is obtained from experiments on various dislocation configurations. It should be noted that data intervals given in the table do not represent the experimental or analysis error but indicate the λ variation along a dislocation line or on several dislocations in a sample. This reveals the influence of the interaction or decoration with point defects as well as others factors such as inhomogeneous bulk doping. Especially, a large local variation is found for dislocations introduced by Zn diffusion/thermal stress in p-GaAs. Furthermore, the data clearly confirm the typical occurrence of smaller defect strengths $\lambda < 0.95$ of fresh glide screw dislocations compared to grown-in, weakly decorated misfit dislocations ($\lambda > 1.26$) in the direct gap III-V materials GaAs and GaAsP. λ values for glide dislocations in GaAs:Si calculated from [69, 72] agree well with our results although these results were obtained on a different geometric configuration. They also show the trend of somewhat higher recombination activity for an α glide dislocation. Several authors [19, 65, 72] found a slightly stronger CL contrast on α- than on β-dislocations in n-GaAs and vice versa in p-type material. Conclusions were drawn concerning the defect-related electronic gap states for these dislocation types. Only relative recombination activity data were given. Recently, essential differences in the recombination activity of polar glide dislocations have been observed in CdTe [40, 63]. There, α dislocations show a localized, defect-related sub-band-gap CL radiation at low temperatures whereas β dislocation are characterized by the usual non-radiative recombination contrast. Since absolute λ values are available from a small number of papers only, further systematic and comparable defect strength measurements remain a current task of combined CL/EBIC experiments.

New and more detailed insight into the defect recombination mechanisms are expected from temperature-

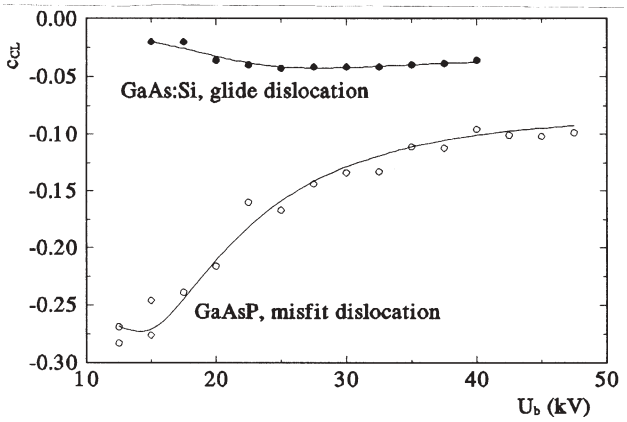

Figure 9. Experimental and fitted CL contrast from a screw type glide dislocation in n-GaAs:Si (fit parameters: $\lambda = 0.95$, $z_D = 1.58\,\mu m$, $L = 0.73\,\mu m$, $\alpha = 1.30\,\mu m^{-1}$, $z_T = 0.03\,\mu m$, $S \rightarrow \infty$) and a misfit dislocation in n-$GaAs_{0.62}P_{0.38}$:Te ($\lambda = 1.78$, $z_D = 0.77\,\mu m$, $L = 0.90\,\mu m$, $\alpha = 1.08\,\mu m^{-1}$, $z_T = 0.12\,\mu m$, $S \rightarrow \infty$).

dependent contrast experiments [19, 65], especially in the low-temperature region below $T = 77$ K where very few results have been published in the past [17, 66]. We have performed panchromatic and spectrally resolved CL experiments between 5 to 300 K. Different behaviors of the dislocation recombination have been found in the III-V materials GaAs and GaP and the II-VI semiconductor CdTe. For the interpretation of these experiments, the defect-related recombination has to be considered in context with the temperature dependence of the bulk recombination rates. Especially, the diffusion length may exhibit a significant variation with temperature [5, 17, 19]. For the present analysis, a basic temperature-dependent recombination-kinetic model including both defect-bound and bulk radiative and non-radiative channels is proposed.

Figure 10 (a) shows typical results of CL contrast measurements as a function of temperature from a surface-parallel misfit dislocation in n-GaP. Contrasts of dislocations perpendicular to the surface behave essentially in the same way. It is seen that as the dark contrast varies rather little with temperature above 70 K, it diminishes quickly below 50 K. In this material the bulk diffusion length L has been found to be only weakly temperature-dependent. This is also reflected by a nearly steady contrast profile half-width of about 6 μm ($c^{**} \approx$ const.). Followed from eqns. 0 and 0, in this case the contrast value may serve as a direct measure for the defect recombination rate R_D:

$$|c_{CL}| \sim \gamma \sim \frac{R_D}{G_0} \approx \frac{\Delta p}{G_0 \tau_D}\ ,\ \gamma = \frac{\tau}{\tau_r} - 1 = \frac{\tau}{\tau_D}. \qquad (15)$$

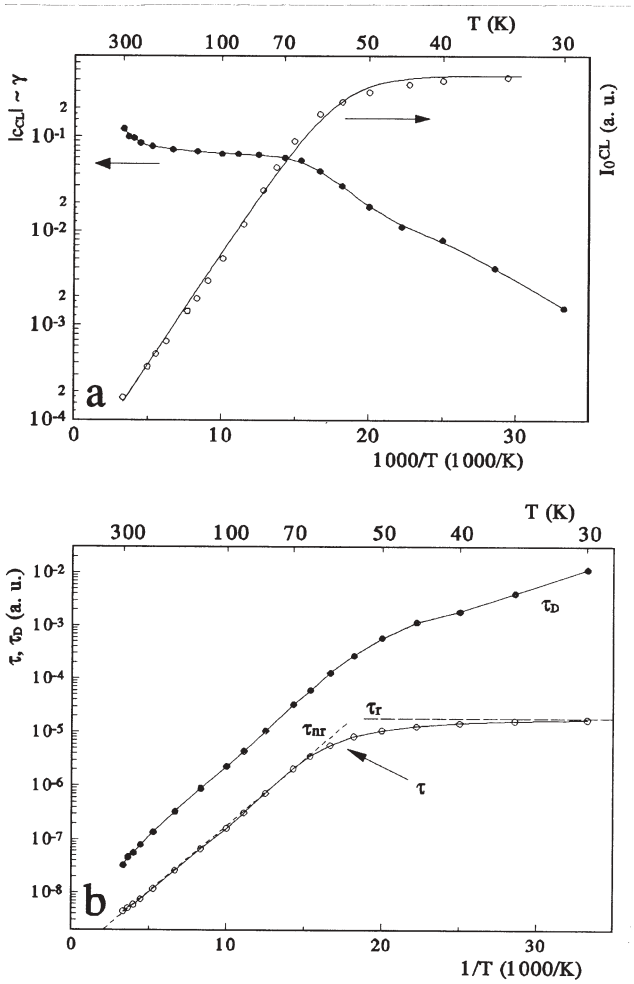

Figure 10. (**a**) Temperature dependence of the CL contrast of a surface-parallel misfit dislocation and the matrix CL intensity in n-GaP ($U_b = 20$ kV), (**b**) Defect and bulk lifetimes as a function of temperature.

From the luminescence intensity $I_0^{CL}(T)$ of the defect- free matrix it is concluded that the bulk recombination is well described by a thermally activated multiphonon process $\tau_{nr} \sim \exp(E_A/kT)$ with $E_A = 47$ meV (cf. [67]) whereas the radiative lifetime τ_r is supposed to be temperature-independent. With the assumption $R_r^D \sim I_D \sim \Delta p$ the temperature dependence of the defect-related lifetime τ_D can be estimated (Figure 10(b)). It changes by more than five orders of magnitude over the investigated temperature range which is interpreted as a distinct variation of the defect-induced recombination properties. The Arrhenius plot implies the participation of thermally activated capture of carriers into shallow defect states and subsequent non-radiative recombination. These states should be of extrinsic rather than intrinsic nature due to the similar temperature dependence of τ and τ_D. In

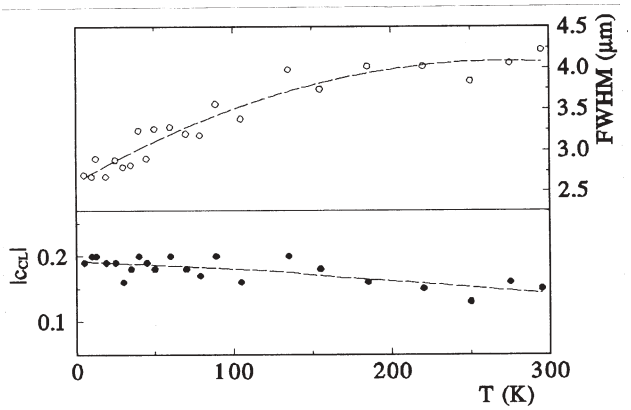

Figure 11. Temperature dependence of CL contrast and profile half-width from a threading glide dislocation in n-GaAs (U_b = 20 kV).

principle, one should be able to describe such a behavior by a model similar to that developed for EBIC on dislocation in Si [71].

On the other hand, on GaAs the observed defect contrast behavior hints at a more complicated correlation between the temperature dependence of dislocation recombination activity and the effect of altered material parameters. Measurements of an individual threading dislocation contrast in the α branch of a microindentation glide rosette show a CL contrast increasing only slightly by 3 % between 300 and 5 K (Figure 11) (see also [17, 19]). Since the diffusion length in GaAs is a strong function of temperature, this effect alone would cause a rapid change in contrast (cf. the theoretical example of Figure 4). Indeed, we also observed a clear increase in the contrast profile half-width from 2.7 μm at T = 5 K to 4.2 μm at room temperature. Therefore, it is inferred that the temperature dependence of defect strength and diffusion length cancel each other to produce only a weakly temperature-dependent contrast. Eliminating the temperature variation of $L(T)$ and $\tau(T)$, the detailed analysis [63] yields a decrease of the actual defect recombination activity ~ $1/\tau_D$ with falling temperature. The deduced thermally activated recombination activity contradicts the interpretation in [17] of quenching of thermal carrier re-emission from a shallow acceptor level.

The results emphasize the relevance of a comprehensive contrast model with inclusion of all material and geometry parameters. This will allow us to combine the straightforward recombination-kinetic analysis with the spatial modelling of the carrier behavior as performed earlier for the room temperature experiments.

Conclusions

The importance of combined SEM-CL/EBIC investigations for the identification and quantitative characterization of recombination-active individual defects in compound semiconductors has been demonstrated. New developments such as advanced realistic analytical and numerical modelling of the defect contrast and investigations in the low-temperature range have been illustrated. The detailed interpretation of derived defect and recombination strength values and the temperature dependence of the material and defect recombination rates remains a challenge in future investigations. For experimental defect studies, the defined preparation of clean or decorated dislocation configurations is a major issue. SEM injection conditions, especially in the low-injection regime, should be carefully considered since it is known that both bulk and defect parameters may be influenced by the carrier injection level and density [2, 68, 71].

Renewed interest is directed to effects of defect-related *radiative* recombination as it has been observed in recent experiments on polar glide dislocations in CdTe at temperatures below 100 K where it gives rise to bright CL contrasts originating from the Te(g) segments [40, 63]. An activation energy of 11 meV for the defect emission determined from the temperature dependence of the local CL spectra is well described by defect-bound excitonic recombination [30]. A further structural and quantitative analysis is in progress.

Finally, other EBIC contrast mechanisms not discussed here such as charge separation at the potential barrier of a charged dislocation connected with one-dimensional conduction along the dislocation line [2, 17, 26] may also be taken into account, especially at low temperatures.

Acknowledgements

This work was partially supported by the research grant no. 1557A0024 from the Ministerium für Wissenschaft und Forschung des Landes Sachsen-Anhalt and a PROCOPE project support no. 312/pro-gg from the Deutscher Akademischer Austauschdienst.

References

[1] Alexander H (1994) What information on extended defects do we obtain from beam-injection methods? Mater Sci Eng B **24**: 1-7.

[2] Alexander H, Dietrich S, Hühne M, Kolbe M, Weber G (1990) EBIC microscopy applied to glide dislocations. phys stat sol (a) **117**: 417-428.

[3] Balk LJ, Kubalek E, Menzel E (1976) Investigations

of as-grown dislocations in GaAs single crystals in the SEM (Cathodoluminescence and electron beam induced voltage). Scanning Electron Microsc 1976; I: 257-264.

[4] Balk LJ, Menzel E, Kubalek E (1980) Microcharacterization of semiconductors by cathodoluminescence (CL) and electron beam induced current (EBIC) techniques. In: Proc. 8th Int. Congress on X-ray Optics and Microanalysis. Beaman DR, Ogilvie RE, Wittry DB (eds.), Pendell Publ. Co., Midland. pp. 613-624.

[5] Bechstein V (1995) Temperaturabhängigkeit des REM-KL-Versetzungskontrastes in III-V-Halbleitern: GaP(n) (Temperature dependence of SEM-CL dislocation contrast in III-V semiconductors: GaP(n)). Diploma thesis. Martin-Luther-Universität, Halle.

[6] Casey Jr HC, Sell DD, Wecht KW (1975) Concentration dependence of the absorption coefficient for *n*- and *p*-GaAs between 1.3 and 1.6 eV. J Appl Phys **46**: 250-257.

[7] Chim WK, Chan DSH, Low TS, Phang JCH, Sim KS, Pey KL (1992) Modelling techniques for the quantification of some electron beam induced phenomena. Scanning Microsc **6**: 961-968.

[8] Christen J, Grundmann M, Bimberg D (1991) Scanning cathodoluminescence microscopy: a unique approach to atomic-scale characterization of heterointerfaces and imaging of semiconductor inhomogeneities. J Vac Sci Technol B **9**: 2358-2368.

[9] Czyzewski Z, Joy DC (1990) Monte Carlo simulation of CL and EBIC contrasts for isolated dislocations. Scanning **12**: 5-12.

[10] Deng H, Steeds JW (1992) Theoretical studies of minority carrier concentration profiles and cathodoluminescence intensities in thin-film materials with different surface recombination velocities and arbitrary excitation density. Semicond Sci Technol **7**: 135-149.

[11] Donolato C (1978/79) On the theory of SEM charge-collection imaging of localized defects in semiconductors. Optik **52**: 19-36.

[12] Donolato C (1979) Spatial resolution of SEM-EBIC images. Solid-State Electron **22**: 797-799.

[13] Donolato C (1983) Evaluation of diffusion lengths and surface recombination velocities from electron beam induced current scans. Appl Phys Lett **43**: 120-122.

[14] Donolato C (1992) A theoretical study of the charge collection contrast of localized semiconductor defects with arbitrary recombination activity. Semicond Sci Technol **7**: 37-43.

[15] Donolato C, Bianconi M (1987) Use of the EBIC contrast profile area for evaluating the recombination strength of dislocations. phys stat sol (a) **102**: K7-11.

[16] Donolato C, Kittler M (1988) Depth profiling of the minority-carrier diffusion length in intrinsically gettered silicon by electron-beam-induced current. J Appl Phys **63**: 1569-1579.

[17] Eckstein M, Habermeier HU (1991) Numerical analysis of the temperature dependence of EBIC and CL contrasts. J Physique IV **1**: C6-23-28.

[18] Fiddicke J, Oelgart G (1985) The importance of the excitation volume for the determination of the minority carrier diffusion length. phys stat sol (a) **87**: 383-389.

[19] Galloway SA, Wilshaw PR, Konkol A (1994) An electron-beam-induced current study of dislocations in GaAs. Mater Sci Eng B **24**: 91-97.

[20] Hergert W (1989) The information radius in electron beam or light beam probing of semiconductors, phys stat sol (a) **111**: K253-257.

[21] Hergert W, Hildebrandt S, Pasemann L (1987) Theoretical investigations of combined EBIC, LBIC, CL, and PL experiments. The information depth of the PL signal. phys stat sol (a) **102**: 819-828.

[22] Hergert W, Pasemann L (1984) Theoretical study of the information depth of the cathodoluminescence signal in semiconductor materials. phys stat sol (a) **85**: 641-648.

[23] Hergert W, Pasemann L, Hildebrandt S (1991) Discussion of the convergence properties of the perturbation series used in the calculation of EBIC- and CL-contrasts. J Physique IV 1: C6-45-50.

[24] Hergert W, Reck P, Pasemann L, Schreiber J (1987) Cathodoluminescence measurements using the scanning electron microscope for the determination of semiconductor parameters. phys stat sol (a) **101**: 611-618.

[25] Herman MA, Bimberg D, Christen J (1991) Heterointerfaces in quantum wells and epitaxial growth processes: Evaluation by luminescence techniques. J Appl Phys **70**: R1-52.

[26] Hess J, Schreiber J, Hildebrandt S, Labusch R (1992) EBIC experiments at dislocations in germanium, phys stat sol (b) **172**: 225-234.

[27] Hildebrandt S, Hergert W (1990) Unified theoretical description of the CL, EBIC, PL, and LBIC contrast profile area of an individual surface-parallel dislocation. phys stat sol (a) **119**: 689-699.

[28] Hildebrandt S, Schreiber J, Hergert W (1991) Recent results in the theoretical description of CL and EBIC defect contrasts. J. Physique IV **1**: C6-39-44.

[29] Hildebrandt S, Schreiber J, Hergert W, Petrov V I (1988) Determination of the absorption coefficient and the internal luminescence spectrum of GaAs and $GaAs_{1-x}P_x$ (x = 0.375, 0.78) from beam voltage dependent measurements of cathodoluminescence spectra in the scanning electron microscope. phys stat sol (a) **110**: 283-291.

[30] Hildebrandt S, Uniewski H, Schreiber J, Leipner HS (1997) Localization of Y luminescence at glide dislocations in cadmium telluride. J. Physique III (in press).

[31] Holt DB, Napchan E (1994) Quantitation of SEM EBIC and CL signals using Monte Carlo electron trajectory

simulations. Scanning **16**: 78-86.

[32] Holt DB, Napchan E, Lazzarini L, Urchulutegui M, Salviati G (1994) Quantitative studies of beam-induced defects in III-V compounds by cathodoluminescence and transmission electron microscopy. Mater Sci Eng B **24**: 130-134.

[33] Holt DB, Napchan E, Norman CE (1989) Calculations for defect strength determinations. Inst Phys Conf Ser **104**: 205-210.

[34] Jakubowicz A (1985) On the theory of electron-beam-induced current contrast from pointlike defects in semiconductors. J Appl Phys **57**: 1194-1199.

[35] Kato T, Nakazawa Y, Matsumoto T (1993) Estimation of grown layer thickness by cathodoluminescence measurement. Jpn J Appl Phys **32**: 5525-5526.

[36] Kaufmann K, Balk LJ (1995) Numerical simulation of electron-beam-induced gate currents in a GaAs MESFET. I. Theory and model. J Phys D **28**: 914-921. II. Numerical and experimental results. ibid. 922-933.

[37] Kittler M, Schröder K-W (1983) Determination of semiconductor parameters and of the vertical structure of devices by numerical analysis of energy-dependent EBIC measurements. phys stat sol (a) **77**: 139-151.

[38] Koch F (1987) Quantitative Bestimmung von Halbleiterparametern mit Hilfe des elektronenstrahlinduzierten Barrierenstromes und der Katodolumineszenzintensität (Quantitative determination of semiconductor parameters by means of electron beam induced barrier current and cathodoluminescence intensity). Thesis. Humboldt-Universität, Berlin.

[39] Koch F, Hergert W, Oelgart G, Puhlmann N (1988) Determination of semiconductor parameters by electron beam induced current and cathodoluminescence measurements. phys stat sol (a) **109**: 261-272.

[40] Leipner HS, Schreiber J, Uniewski H (1997) Dislocation luminescence in the compound semiconductor cadmium telluride. Scanning Microsc, in press.

[41] Löhnert K, Kubalek E (1984) The cathodoluminescence contrast formation of localized non-radiative defects in semiconductors. phys stat sol (a) **83**: 307-314.

[42] Luke KL (1994) Choice of a range-energy relationship for the analysis of electron-beam-induced current line scans. J Appl Phys. **76**: 1081-1091.

[43] de Meerschman C, Sieber B, Farvacque J-L, Druelle Y, Microscale characterisation of epitaxial semiconducting homolayers, I. Cathodoluminescence, Microsc Microanal Microstruct **3** (1992) 483-499; II. Electron beam induced current. ibid. 501-516.

[44] Munnix S, Bimberg D (1988) Carrier injection in semiconductors with position-dependent band structure: electron-beam-induced current at heterojunctions. J Appl Phys **64**: 2505-2514.

[45] Pasemann L (1981) A contribution to the theory of the EBIC contrast of lattice defects in semiconductors. Ultramicrosc **6**: 237-250.

[46] Pasemann L (1991) A contribution to the theory of beam-induced current characterization of dislocations. J Appl Phys **69**: 6387-6393.

[47] Pasemann L (1994) Theory of electron-beam-induced current and cathodoluminescence imaging of crystal defects: some new results. Mater Sci Eng B **24**: 15-22.

[48] Pasemann L, Blumtritt H, Gleichmann R (1982) Interpretation of the EBIC contrast of dislocations in silicon. phys stat sol (a) **70**: 197-209.

[49] Pasemann L, Hergert W (1986) A theoretical study of the determination of the depth of a dislocation by combined use of EBIC and CL technique. Ultramicrosc **19**: 15-22.

[50] Petrov VI (1992) Cathodoluminescence scanning microscopy. phys stat sol (a) **133**: 189-230.

[51] Petrov VI, Gvozdover RS (1991) Spatial resolution of cathodoluminescence scanning electron microscopy of semiconductors. Scanning **13**: 410-414.

[52] Pey KL, Chan DSH, Phang JCH (1993) A numerical method for simulating cathodoluminescence contrast from localised defects. Inst Phys Conf Ser **134**: 687-692.

[53] Pey KL, Phang JCH, Chan DSH (1995) Cathodoluminescence contrast of localized defects. Part I. Numerical model for simulation. Scanning Microsc **9**: 355-666. Part II. Defect investigation. ibid. 367-380.

[54] Phang JCH, Pey KL, Chan DSH (1992) A simulation model for cathodoluminescence in the scanning electron microscope. IEEE Trans Electron Devices **39**: 782-791.

[55] Puhlmann N, Oelgart G, Gottschalch V, Nemitz R (1991) Minority carrier recombination and internal quantum yield in GaAs:Sn by means of EBIC and CL. Semicond Sci Technol **6**: 181-187.

[56] Reimer L (1995) Monte Carlo simulation MOCASIM. Software manual. Prof. Dr. L. Reimer, Alte Schanze 22, D - 48159 Münster, Germany.

[57] Rossin VV, Sidorov VG (1986) Reabsorption of recombination radiation in semiconductors with high internal quantum efficiency. phys stat sol (a) **95**: 15-40.

[58] Schönauer W, Schnepf E, Müller H (1985) The FIDISOL program package. Internal report no. 27/85. Universität Karlsruhe. Rechenzentrum, Postfach 6980, D - 76049 Karlsruhe, Germany.

[59] Schreiber J, Hergert W (1989) Combined application of SEM-CL and SEM-EBIC for the investigation of compound semiconductors. Inst Phys Conf Ser **104**: 97-107.

[60] Schreiber J, Hergert W, Hildebrandt S (1991) Combined application of SEM-CL and SEM-EBIC for the investigation of compound semiconductors. Appl Surf Sci **50**: 181-185.

[61] Schreiber J, Hildebrandt S (1994) Basic dislocation contrasts in SEM-CL/EBIC on III-V semiconductors. Mater Sci Eng B **24**: 115-120.

[62] Schreiber J, Hildebrandt S, Leipner HS (1993) Studies on carrier recombination at dislocations in compound semiconductors by combined SEM-CL/EBIC measurements. phys stat sol (a) **138**: 705-713.

[63] Schreiber J, Hildebrandt S, Uniewski H, Bechstein V (1996) Investigation of the low-temperature CL contrasts of dislocations in compound semiconductors. Mater Sci Eng B **42**: 24-31.

[64] Selberherr S (1984) Analysis and Simulation of Semiconductor Devices, Springer-Verlag, Berlin. pp. 149-285.

[65] Sieber B, Farvacque JL, Miri A (1993) Cathodoluminescence evidence of the relative position of As(g) and Ga(g) dislocation-related energy bands in gallium arsenide. phys stat sol (a) **138**: 673-680.

[66] Steckenborn A, Münzel H, Bimberg D (1981) Cathodoluminescence lifetime pattern of GaAs surfaces around dislocations. J Lumin **24-25**: 351-354.

[67] Stegmann R, Kloth B, Oelgart G (1982) The temperature dependence of luminescence intensity on $GaAs_{1-x}P_x$:N. phys stat sol (a) **70**: 423-431.

[68] Tajima M, Kawate Y, Toba R, Warashina M, Nakamura A (1996) Microscopic photoluminescence mapping of Si-doped GaAs around dislocations at low temperatures. Inst Phys Conf Ser **149**: 257-262.

[69] Weber G, Dietrich S, Hühne M, Alexander H (1989) EBIC investigations of dislocations in GaAs. Inst Phys Conf Ser **100**: 749-754.

[70] Werner U, Koch F, Oelgart G (1988) Kilovolt electron energy loss distribution in Si, J Phys D **21**: 116-124.

[71] Wilshaw PR, Booker GR (1985) New results and an interpretation for SEM EBIC contrast arising from individual dislocations in silicon. Inst Phys Conf Ser **76**: 329-336.

[72] Wosinski T, Zozime A, Rivière A, Vermeulin C (1994) EBIC investigations of α and β dislocations in GaAs. phys stat sol (a) **142**: 347-355.

[73] Wu CJ, Wittry DB (1978) Investigation of minority-carrier diffusion lengths by electron bombardment of Schottky barriers. J Appl Phys **49**: 2827-2836.

[74] Yacobi BG, Holt DB (1990) Cathodoluminescence of Inorganic Solids. Plenum Press, New York. pp. 121-229.

Discussion with Reviewers

T. Sekiguchi: As for the experimental point of view, the excitation energy (E) dependence is somewhat ambiguous. It comes from the different behavior of total number of generated carriers and their density on the excitation energy (E). If we accept the uniform generation sphere model and the generation radius is proportional to $E^{1.75}$, the excess carrier density is proportional to $E^{-4.25}$, while total number of excess carriers to E. Which parameter is required to be constant, the density or the total number of generated carriers?

Please suggest us how experimental procedure should be done.

Authors: From a physical perspective, the experiments should be performed at a small constant excess carrier density in the low injection range at the defect or in the sample region to be investigated. However, the exact evaluation of the excitation level inside the sample is not straightforward. Values for the carrier density q calculated on the basis of simplified generation models can only be a rough estimate. $q(\boldsymbol{r})$ may vary by several orders of magnitude over $\boldsymbol{r}$ and the material parameters L and D. Usually, the maximum of the $q(\boldsymbol{r})$ distribution must be calculated for the correct semiconductor parameters and realistic generation to determine the injection level.

Experimentally, the validity of the low injection regime should be proved *for each specimen* by inspecting the linear variation of the CL and EBIC signal with beam current I_b at a given beam voltage $U_b = E/e$. Also, the signal should be equal for focused and defocused beam, respectively. In practice, beam voltage dependent experiments have been performed at *constant beam power* $P = U_b\, I_b$ which must be small enough to fulfil the low injection condition even for the smallest U_b (typically $P < 5$ ... 20 μW) [24, 29, 39]. The obtained CL and EBIC signals are then normalized to the total generation rate G_0 being approximately constant except for a weakly U_b-dependent backscattering correction. It should also be kept in mind that the low injection condition may be different for defect recombination paths. This can be checked by measuring $c(I_b)$ at U_b = const.

T. Sekiguchi: Do you have some idea about the value of λ and the physical parameter of dislocation (Table 2)?

Authors: As the defect strength λ is given in first order approximation by 0, it depends on the ratio of τ/τ_D of lifetimes for defect and matrix recombination paths as well as on the dislocation radius r_D. The further interpretation of λ requires the implementation of a dislocation model which calculates these quantities on the basis of the recombination kinetics. Various models for defect recombination controlled by the dislocation charge [71] or based on the Shockley-Read-Hall recombination statistics [76] have been successfully employed for Si. However, they should be applied to the extracted defect strength rather than to the contrast as it has been well demonstrated in one of your recent papers [77]. The development of recombination-kinetic models for dislocations in compound semiconductors is the subject of current investigations [63, 65]. Usually, their application will

require temperature or beam current dependent contrast measurements. The recombination mechanisms are expected to be more complex than in Si, for example if excitonic transitions are involved.

J.C.H. Phang: It has been shown in [75] that various semiconductor parameters may be extracted entirely from CL experimental data by varying the incident beam energy. Is it necessary to use both CL and EBIC data to determine the parameters as suggested in Table 1?
Authors: The correlation of L and α in the U_b dependence of the CL matrix signal means that the global minimum of the sum of least squares in parameter space is a very shallow one. You have demonstrated that it may still be possible to find this minimum by using sophisticated and extensive minimization techniques. However, it is doubtful if this can be achieved for any limited set of realistic data couples with both statistical and systematic errors. For example, it is possible to fit the data in Fig. 8 of [75] using L and α couples being about four times larger than the values given (thereby adjusting the other parameters as well) which leads to an increase in the sum of least squares of only about 0.1 %. Therefore, one should also look for alternatives to determine L from CL data, for example, using the contrast profile half-width. It is obvious, however, that both CL and EBIC experiments are needed if the *total* as well as the *radiative* defect strengths λ and λ_r are to be characterized, for example due to the occurrence of a defect-related spectral CL emission.

Additional References

[75] Chan DSH, Pey KL, Phang JCH (1993) Semiconductor parameters extraction using cathodoluminescence in the scanning electron microscope. IEEE Trans Electron Devices **40**: 1417-1425.

[76] Kittler M, Seifert W (1993) On the origin of EBIC defect contrast in silicon. A reflection on injection and temperature dependent investigations. phys stat sol (a) **138**: 687-693.

[77] Kusanagi S, Sekiguchi T, Sumino K (1995) Energy states of deformation-induced dislocations in silicon crystals. Mater Sci Forum **196-201**: 1195-1200.